High-Voltage High-Frequency Arbitrary Waveform Multilevel Generator for DBD Plasma Actuators

Article *in* IEEE Transactions on Industry Applications · March 2015

DOI: 10.1109/TIA.2015.2409262

4 authors:

Filopimin Dragonas
Arca Technologies
7 PUBLICATIONS **28** CITATIONS
SEE PROFILE

Gabriele Neretti
University of Bologna
54 PUBLICATIONS **403** CITATIONS
SEE PROFILE

P. Sanjeevikumar
Aalborg University
346 PUBLICATIONS **715** CITATIONS
SEE PROFILE

Gabriele Grandi
University of Bologna
144 PUBLICATIONS **2,676** CITATIONS
SEE PROFILE

This article has been accepted for publication in a future issue of this journal, but has not been fully edited. Content may change prior to final publication. Citation information: DOI 10.1109/TIA.2015.2409262, IEEE Transactions on Industry Applications

High-Voltage High-Frequency Arbitrary Waveform Multilevel Generator for DBD Plasma Actuators

Filopimin A. Dragonas, Gabriele Neretti, Padmanaban Sanjeevikumar, Gabriele Grandi, *Senior Member*, *IEEE*
Dept. of Electrical, Electronic, and Information Engineering, *Alma Mater Studiorum* - University of Bologna, Italy.

***Abstract*—A high-voltage high-frequency single-phase arbitrary waveform voltage generator able to supply a wide range of plasma reactors is proposed in this paper. The generator structure is based on the cascaded H-bridge multilevel topology, including 24 H-bridge basic modules with the capability of 49 output voltage levels. The individual H-bridge dc supply (600V) is provided by a flyback converter fed by a low-voltage (12V) dc battery. In this way, the input isolation of the ±14.4kV maximum output voltage is realized in a simple and effective manner, and a portable device is obtained. The multilevel generator has been tested by supplying a dielectric barrier discharge (DBD) fluid-dynamic plasma actuator with different voltage waveforms, pointing out a wide and interesting set of results in terms of output plasma currents, and a first comparison has been carried out with respect to a conventional AC sinusoidal generator. A simplified circuit model has been introduced for the DBD plasma actuator, and the whole system has been numerically implemented by Simulink of Matlab. The simulation results are in good agreement with the experiments.**

I. Introduction

High voltage generators with low output current represent a small fraction of the broad spectrum of power supply devices currently present on the market. Nevertheless, there is a large number of applications that require such type of equipment and the demand is strong and continuously increasing. Typical cases with high-voltage but limited output current are plasma reactors operating with dielectric barrier discharges (DBDs) [1], [2].

The non-thermal plasma produced by a DBD is currently being experimented in different research fields and industrial processes [3], [4]. The relative low temperature of heavy particles that coexist with high energetic electrons and reactive radicals, make this type of plasma very attractive for engineering purposes. The main application domains are the following:

- plasma etching in microelectronics [5];
- surface treatment to increase dyeability, wettability and adhesion [6];
- sterilization of surfaces and gases from bacteria, parasites and molds [7];
- abatement of pollutants and volatile organic compounds present in combustion processes and cooking activities [8];
- ozone production [9];
- food treatment by using pulsed electric fields (PEF) and non-thermal pasteurization [10], [11];
- plasma biology and plasma medicine for skin, teeth and wounds treatment [12], [13];
- electro-fluid-dynamic actuators (EHD) for active flow control [14].

All the cases mentioned above require high voltages and high frequencies, and they usually make use of power supplies that were not originally designed for such specific applications. Two of the most common types of generators used in these cases are either power amplifiers with high voltage transformers or resonant switching converters. Both of these designs have some disadvantages. First, these systems are usually bulky devices built for high power applications that are inefficient when coupled with capacitive loads (i.e. previously presented applications). In particular, resonant converters have to be fine tuned in order to optimize their performance. The optimum operating point is unique and can significantly change as a result of small load and connection variations. Furthermore, conventional power supplies can only generate a restricted number of voltage waveform types, essentially sinusoidal. However, the effect of the waveform shape in DBD fluid-dynamics actuators is currently being studied [14]. Hence there is strong interest on trying new voltage waveforms which could enhance the induced speed both by increasing the net thrust and both by modifying the surface charge build-up phenomenon [16], [17].

In this a different approach to realize high-voltage high-frequency power supply is proposed, based on the multilevel (ML) voltage source converter technology [18]. Different ML topologies have been proposed in last decades. In particular, the modular multilevel converter (MMC) topology offered the possibility to exploit the ML technology for both motor drives [19] and transformerless grid-connected applications [20].

Hybrid and asymmetrical solutions has been proposed [21] and, more recently, also the neutral-point clamped (NPC) topology has been introduced for large motor drives, solving the problem of balancing the neutral-point potential [22].

Among the different ML topologies, the cascaded H-bridge configuration topology offers the advantage of simple modularity, being built on the duplication of one elementary conversion module (H-bridge). Due to this design modularity and flexibility, the usage of standard electrical components and integrated circuits is possible even when generating high voltage output waveforms [23]. Furthermore, being a voltage-source converter type, the output waveform is practically unaffected by load changes i.e. no matching impedance is required. This characteristic is particularly useful for DBD plasma actuators. For this reason, a single-phase ML converter topology consisting of 24 cascaded H-bridge modules, generating up to 49 output voltage levels, and leading to a virtually infinite number of arbitrary output waveforms is proposed in this paper (Fig. 1). The main drawback lies in the needs of isolated dc supplies for each H-bridge module, requiring high-voltage isolation among them. This problem has been preliminary solved by introducing isolated low-voltage batteries and flyback step-up choppers, making possible the portability of the proposed high-voltage high-frequency generator (Fig. 1).

This article has been accepted for publication in a future issue of this journal, but has not been fully edited. Content may change prior to final publication. Citation information: DOI 10.1109/TIA.2015.2409262, IEEE Transactions on Industry Applications

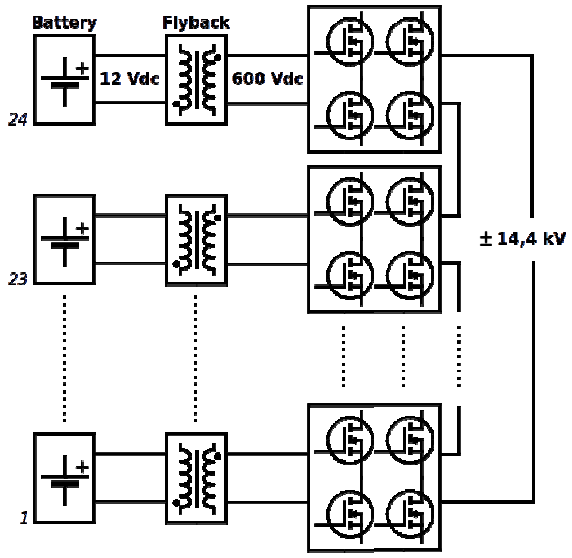

Fig 1. Block diagram of the 24-level cascaded H-bridge inverter.

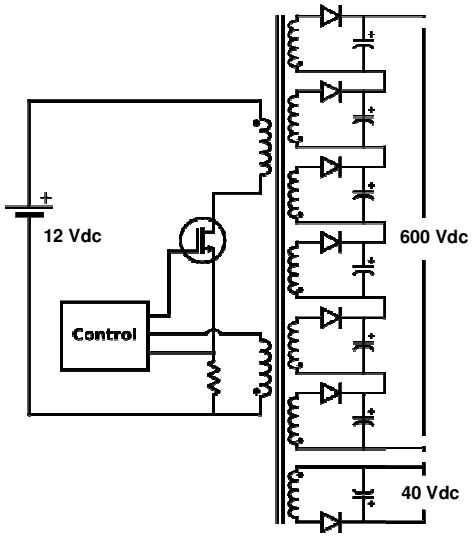

Fig 2. Topology of the flyback converter supplying each H-bridge module.

A complete overview of the multilevel waveform generator is presented in the following sections, starting from the analysis of a single H-bridge module. Furthermore, on the basis of the experimental results, a simplified circuit model of the DBD plasma actuator has been introduced. The whole conversion system has been numerically implemented by the Simulink tool of Matlab, obtaining simulation results in good agreement with the corresponding experiments.

II. System Description

This Section introduces the hardware design specifications and focuses on some key points of the implementation. As mentioned above, a great advantage of using the cascaded multilevel topology lies in its modular nature. The high-voltage output waveform can be subdivided into equal voltage steps that are generated by elementary modules (Fig. 1). In this paper, the desired peak-to-peak voltage was 28.8 kV (±14.4 kV) which has been shared into 24 levels. The resulting peak-to-peak output voltage range for each H-bridge module is 1.2 kV (±600 V). The control algorithm capable of generating the arbitrary high-voltage waveforms with an output frequency up to 20 kHz is explained in next Section.

The basic H-bridge module consists in a voltage step-up input section, also providing galvanic isolation, and a H-bridge output section, providing the required voltage levels.

Voltage step-up and input isolation are implemented by the multi-stage flyback converter with HF transformer, represented in the simplified scheme of Fig. 2. The primary source is a battery providing a dc voltage supply of 12 V. In order to have a stable flyback output, the secondary voltage is regulated in the closed-loop control mode. For this purpose, an auxiliary secondary feedback winding is needed to provide voltage measurement in addition to the Mosfet current sensing. The regulation is managed by a UC3845 integrated circuit which is a current mode PWM controller. The PWM firing signal supplies the Mosfet gate which periodically turns on to provide the necessary current to the flyback transformer. The switching frequency is set to 80 kHz. The 600 V dc-bus voltage has been evenly split among 6 series-connected windings which provide the full voltage amplitude. At last a seventh secondary winding set to 40 V provides power to low power auxiliary circuits. The power deliverable by each flyback in continuous mode is 20 W. The rated power of the multilevel generator is thus 480 W (i.e. 20 W by 24 modules). In the next Section "Experimental results" this power is compared with the one effectively feeding the plasma actuator, allowing to the determination of the efficiency of the whole supply system.

The flyback converter provides the necessary voltage to sustain the dc bus used by the inverter. The inverter used is a PS22A74 model which belongs to the intelligent power modules family produced by Mitsubishi Semiconductors [24]. These modules are integrated circuits which come in a convenient dual in-line package and comprise of both the power semiconductor components, i.e. IGBTs, as well as the drivers. The maximum rated voltage of the specific model is 1200 V while the operational voltage is 600 V. The module can support continuous output currents up to 15 A though only a fraction of that quantity is used in this application, improving the converter reliability. In fact, the DBD load is characterized by a "pulsating" behavior, related to the continuous formation, development, and shutdown of current streamers. Even though the RMS value of the current supplying the DBD actuator is low, very high current peaks can be achieved. A high value of the IGBTs rated current guarantees the correct development of the discharge, providing a large amount of instantaneous power to the DBD load with a safety current margin.

The power module consists in a full three-phase bridge, but only two legs are used in this case (H-bridge), leaving the third leg eventually as a back-up. The control signals are transferred to the power module through the use of optic fibers. This choice was primarily made for safety precautions as complete galvanic isolation had to be guaranteed between the control electronics and the power circuitry.

As known, the dc power supplies of the cascaded H-bridge multilevel topology need to be isolated each other. The most common solution to this problem is to use separate isolated dc sources for each H-bridge. It is typically implemented by using a transformer where the main power supply source is con-

This article has been accepted for publication in a future issue of this journal, but has not been fully edited. Content may change prior to final publication. Citation information: DOI 10.1109/TIA.2015.2409262, IEEE Transactions on Industry Applications

nected to the primary winding and individual secondary windings feed each H-bridge separately. Galvanic isolation has to be provided between the secondary windings and the primary for the peak multilevel output voltage. In this implementation it would have been almost 15kV which would have lead to using a large and bulky transformer. Instead, by using the batteries as dc sources, a more compact solution was found which provides isolation and also makes the waveform generator a portable device.

III. Control Method

The control of the multilevel inverter is handled by an ATmega2560 microcontroller unit (MCU) produced by Atmel. Clocked at 16 MHz with a flash memory of 256 kB this MCU has 54 digital I/O pins (note that a minimum of 48 was required). An Arduino Mega 2560 single board programmer has been used to upload the code to the MCU. The assembly programming language was preferred over a higher level language (e.g. C) because the latter generated timing issues in the control signals due to the delays introduced by single line of code.

A. Generation of firing signals

As described in previous Section, the proposed multilevel generator is composed by 24 separate H-Bridge inverters. In order to minimize the number of control signals and to prevent any flaws in the switching sequences, dead time for each IGBT driver has been hardware implemented on the PCB board. Thus instead of using 4 control signals, one for each IGBT, only 2 control signals are needed to be transferred from the MCU to a single H-bridge board, one for each switching leg. Summarizing, the total number of digital control signals is 48, and the available output voltage levels are 49, including zero.

Considering the large number of control signals, any PWM control scheme would present serious synchronization challenges in its implementation and would require significant processing effort from the control system. On the other hand the great number of voltage levels allows the generation of a very well defined output waveform. This advantage can be exploited by the use of a control method that simply sets the state of each elementary module and the appropriate duration without worrying about any type of modulation. This method known as “Bit banging” has the benefit of being straightforward in its implementation, proving as many control signal instances as needed while keeping the processing requirements low. This type of code requires direct port manipulation I/O pins of the MCU.

Each port is controlled by a register that sets the logical state of the respective pin to either HIGH or LOW. The registers are 8 bit long which means that they simultaneously set the state of 8 control signals, therefore a total of 6 registers are needed for the complete multilevel system. PortX refers to each register and its value is specified in binary format. The other important line of code shown in this example is the delayMicroseconds(X) function which basically holds the set register values (i.e. control signal states) for a given time (μs). Thus by controlling the state of the registers and the time it takes between each variation any arbitrary waveform with a voltage resolution of 600 V can be generated.

An example of the programming code to produce a 5-level square wave at 10 kHz is the following:

```
PortA=B00000011;
PortB=B00000000;
delayMicroseconds(50);
PortA=B00000000;
PortB=B00000011;
delayMicroseconds(50).
```

B. Input power balancing

The development of the control scheme should to take into account that the system is powered by batteries and thus a way of balancing the discharge has to be implemented in order to extend the battery life and maximize the generator usage.

In order to solve this problem, a rotation of the output levels among the H-bridge modules has been introduced. This algorithm has been implemented on the control board in order to circularly change the switch on time of the H-bridge after each fundamental period. In this way, after 24 fundamental periods the total on time for each h-bridge is perfectly equal, and the role of each H-bridge is the same of each other. The application of this simple balancing technique substantially increased the batteries life, making possible the usage of the multilevel generator for almost one full hour of experiments.

IV. Experimental Results

The prototype of the multilevel generator has been realized and tested by supplying a DBD fluid-dynamic actuator (non-thermal plasma reactor). The scheme of the EHD actuator is shown in Fig 3. A 4 mm thick plexiglass slab has been used as dielectric material. The two electrodes are made of copper strips 200 mm wide (z-direction), 12 mm large (x-direction) and 0.04 mm thick (y-direction). No horizontal gap between dielectric sheet and electrodes is present. The upper electrode is connected to the high voltage source, the lower one is grounded. Both electrodes are exposed to the air. In this way two symmetric plasma regions are generated on the two faces of the dielectric surface in front of the electrodes.

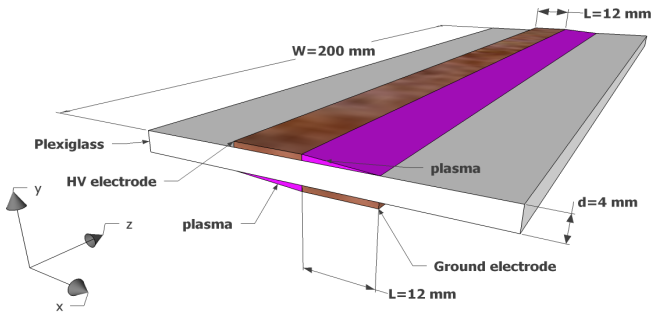

Fig. 3. Schematic drawing of the DBD plasma actuator.

This article has been accepted for publication in a future issue of this journal, but has not been fully edited. Content may change prior to final publication. Citation information: DOI 10.1109/TIA.2015.2409262, IEEE Transactions on Industry Applications

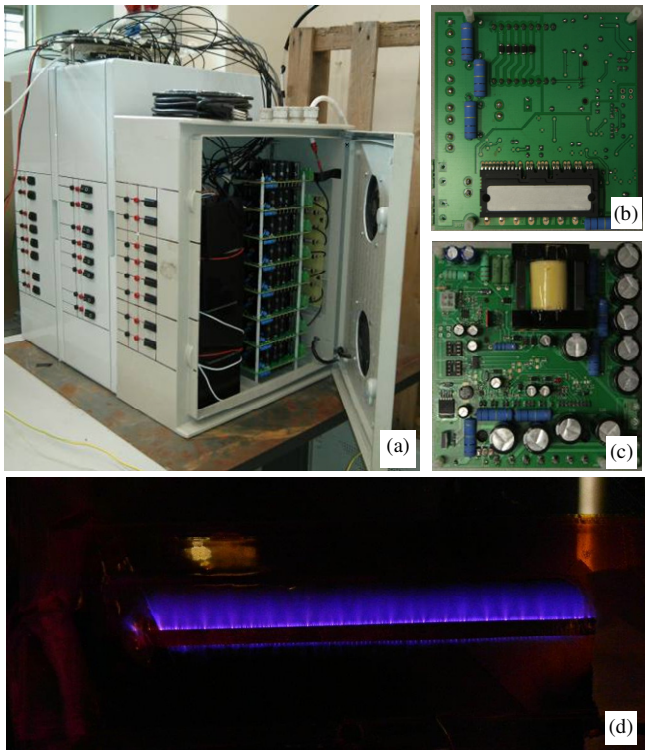

Fig. 4. Experimental setup: (a) multilevel generator realized with 3 racks with 8 modules each, (b) back and (c) front views of one of the 24 flyback/ H-bridge board, (d) top view image of the DBD plasma actuator (load).

In Fig. 4 are shown some pictures of the experimental setup. Note that the 24 H-bridge modules and the corresponding flyback supply choppers have been realized in 24 isolated boards (Figs. 4b and 4c), each one connected to the digital control unit by 2 optic fibers. The 24 boards are grouped in 3 racks (towers) of 8 boards each, including 8 dc supply batteries (Fig. 4a). The control unit has been left outside of the 3 racks to provide a safe remote control of the multilevel generator by the multiple optic fibers connection.

The time behavior of voltage $v(t)$ applied to DBD electrodes have been measured by a Tektronix P6015A capacitive compensated high voltage probes, with a bandwidth of 75 MHz. The corresponding discharge current $i(t)$ has been sensed by a Tektronix TCP312 Hall current probe, with a bandwidth of 100 MHz.

In Fig. 5 are presented the results obtained by supplying the DBD actuator with different types of symmetric and asymmetric voltage waveforms (5 kHz), applying the whole positive and negative available voltage (±14.4kV). The DBD load essentially consists in a series R-C non-linear circuit load, as examined in more details in the following section.

Fig. 5a shows a basic rectangular voltage waveform, 5 kHz, ±14.4 kV. As expected, a current pulse can be observed only in correspondence to each voltage commutation. Positive and negative current peaks are almost symmetric with amplitude of about ±1.6 A. A detailed zoom is given if Fig. 6.

In Fig. 5b a triangular symmetrical voltage waveform is considered, 5 kHz, ±14.4 kV. In this case, each voltage step includes two basic levels (1.2 kV). As expected, positive and negative current pulses appear during the positive and negative voltage slope, respectively, with an (average) amplitude of about ±0.08 A.

Fig. 5c shows a saw-tooth voltage waveform (negative slope), 5 kHz, ±14.4 kV. In this case, one basic voltage level has been used for each voltage step (600 V), corresponding to the maximum voltage resolution. Negative current peaks are almost halved with respect to previous case (Fig. 5b), being the voltage steps halved as well. Large positive current peaks

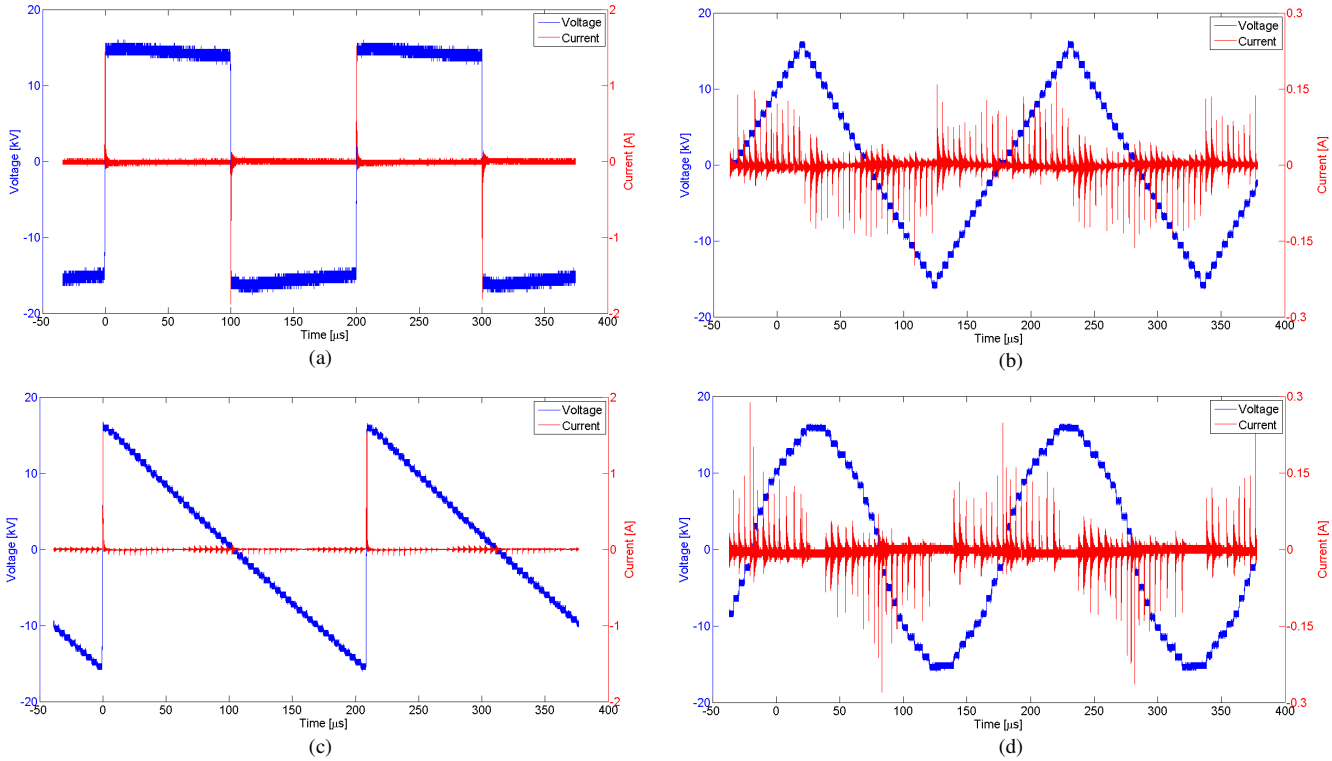

Fig. 5. Different output voltage profiles and corresponding DBD currents: (a) rectangular, (b) triangular, (c) saw-tooth, and (d) sinusoidal waveforms.

This article has been accepted for publication in a future issue of this journal, but has not been fully edited. Content may change prior to final publication. Citation information: DOI 10.1109/TIA.2015.2409262, IEEE Transactions on Industry Applications

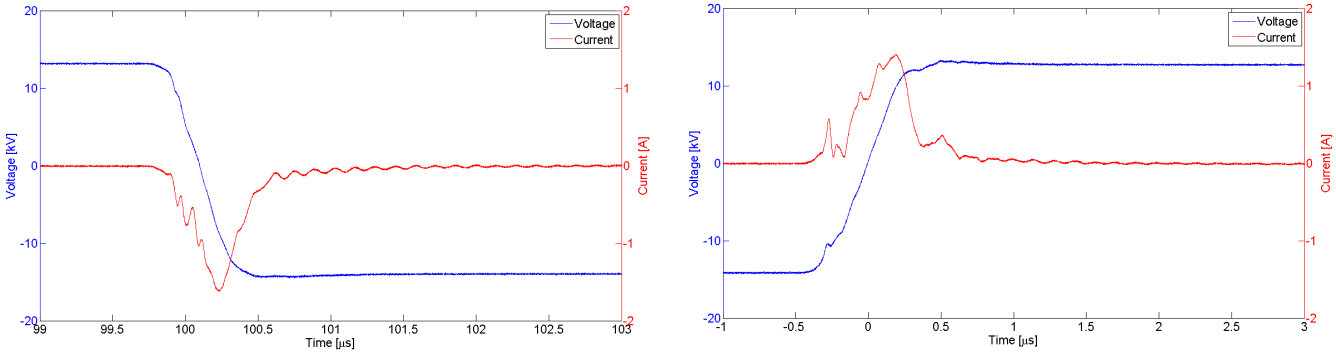

Fig. 6. Experimental results: zoom of a ±14.4 kV falling and rising voltage transients, (a) and (b), respectively.

of about 1.6 A occur during full positive voltage transitions, corresponding to peaks of the rectangular waveform (Fig. 5a).

Fig. 5d shows a nearly-sinusoidal voltage waveform, 5 kHz, ±14.4 kV. A non uniform distribution of positive and negative current peaks amplitude in the fundamental period can be observed, with greater values across the zero crossings of voltage sinusoid, and lower values around the positive and negative voltage flats, as expected.

In general, it can be pointed out that the knowledge of current time behavior obtained by different voltage waveforms is fundamental to study and analyze the discharge formation and its interaction with the surrounding neutral fluid (air in these experiments).

In order to make a better insight of the discharge behavior, a comparison between the voltage-current time characteristics obtained by using the sinusoidal multilevel waveform and by utilizing a conventional AC continuous supply system has been carried out (Fig. 7). The conventional AC generator is implemented by a sinusoidal signal source, a low voltage Elgar AC power amplifier (rated power 3 kVA) and a ferrite step-up transformer. A 15 kV peak, 5 kHz sinusoid has been produced. As widely reported in literature, when a sinusoidal waveform is applied to a DBD actuator, the time behavior of the current follows the periodic behavior of the voltage with the superposition of current peaks corresponding to the phases in which plasma is randomly generated. These regions roughly correspond to the time intervals in which the module of the applied voltage is increasing. The comparison shown in Fig. 7 points out that current peaks detected when the multilevel is used as voltage source, are about three times higher with respect to those produced when the AC conventional power supply is utilized. With the multilevel sine waveform, current streamers are not generated in a randomized way as in the AC sine waveform. Streamers are forced to form solely when a voltage step is applied and are thus spaced in time. A comparable amount of charges must be carried to the plasma in a confined time with respect the AC waveform. This corresponds to a high quantity of charges delivered to the discharge in the form of 'packages', leading to higher current peaks. The aspects already discussed are supported by a substantial equality in the amount of active power delivered to the discharge by using the two waveforms. Considering that the multilevel sine wave mimics the conventional AC sine wave, and taking into account that the active power is

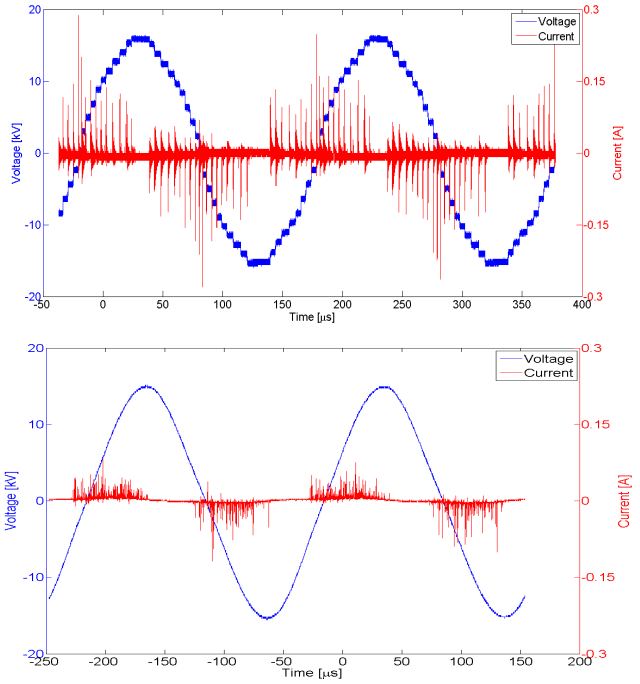

Fig 7. Output voltage profiles and corresponding DBD currents for sinusoidal multilevel waveform (top) and conventional AC sinusoid (bottom).

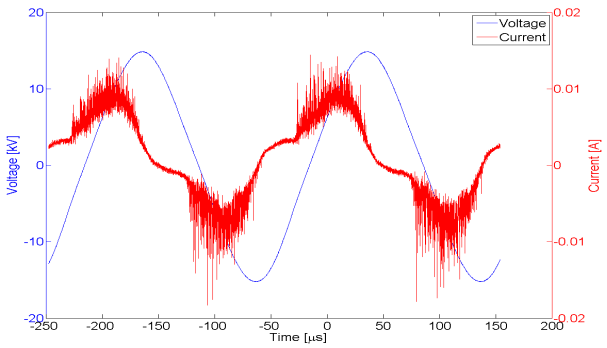

Fig 8. Output voltage profiles and corresponding DBD currents (zoomed) for the conventional AC sinusoid: acquisition in 'average mode'.

about the same in the two cases, it can be argued that a similar overall amount of charges is delivered to the discharge by the two voltage waveforms. The two supply systems seem thus to change the way by which charges feed the discharge, not their amount.

This article has been accepted for publication in a future issue of this journal, but has not been fully edited. Content may change prior to final publication. Citation information: DOI 10.1109/TIA.2015.2409262, IEEE Transactions on Industry Applications

Another important feature is related to the plasma formation within a period of the applied voltage waveform. As already discussed, when an AC voltage source is utilized to supply a DBD actuator, two plasma regions are detected within the voltage period. This behavior is made even more clear by observing Fig. 8, representing the same voltage-current time characteristic already reported in the bottom plot of Fig. 7. In Fig. 8, acquisitions have been performed by setting the scope in the 'average mode' (exponential averaging, Yokogawa DL1740). The resulting waveforms have been calculated by using the following expression:

$$A_n = \frac{1}{N}\left[(N-1)A_{n-1} + X_n\right], \tag{1}$$

where A_n is the value obtained after n-th averaging, X_n is the n-th measured value, and N is the attenuation constant. The attenuation constant N has been fixed equal to 16, the record length set to the maximum value, 500 k, and the signals have been acquired for 10 seconds. The sample rate of the scope is 500 MS/s.

Fig. 8 clearly points out that the current is constituted by an AC component due to the capacitive nature of the DBD actuator, with the superposition of the two abovementioned time intervals in which the discharge is ignited.

When the multilevel generator is used to feed the discharge, the regions in which plasma is produced are not clearly detectable. This aspect is currently being investigated and will be presented soon in a next scientific paper. Up to now, the ability of the multilevel generator to produce an arbitrary waveform used to ignite a DBD has been widely described.

Another important parameter related to the voltage source is the output power. Conventional AC generators utilized to supply DBD plasmas are usually characterized by electrical efficiencies below the 40%. This means that more than half of the input electrical power is not delivered to the load. The low efficiencies are mainly due to power losses in the step-up transformers and related to the impedance mismatch between the voltage source and the load. As far as a DBD actuator is a time dependence load, the resonance condition, in which the highest efficiency is reached, is not easy to achieve. For a given actuator geometry and thus for a given actuator capacitance, only one value of resonance frequency exists. As already emphasized, the multilevel generator is unaffected by any matching impedance requirements. In order to verify this feature and to evaluate the multilevel generator efficiency, several actuators built on the basis of the geometry described in Fig. 3 and characterized by different spanwise lengths W have been adopted. The spanwise length has been increased starting from 0.1 m up to 1.5 m. The multilevel generator was able to correctly supply the discharge, as the shape of the applied waveform was unaffected by the actuator length. Active output powers up to 320 W have been measured, corresponding to the maximum input power of 480 W, leading to an efficiency of about 66%. Conventional AC generators were not able to supply actuators with different spanwise lengths. Both the abovementioned 'home made' AC power source and the commercial Minipulse 6 power supply, characterized by a nominal input power of 800 W, have been used. Despite the high rated power of these two AC generators, they were not able to fully feed the discharge when the resonance conditions were not achieved. This condition roughly corresponds, at 5 kHz, to actuator lengths in the range 0.15–0.25 m. Even in the resonance condition, efficiencies were below 40%.

V. Modeling and Simulations

In order to get a simplified functional model in working conditions (plasma activated), a series RC equivalent circuit is considered.

A parallel plate capacitor having a surface ranging from one to two times the area of the metallic electrodes can be considered for the evaluation of the capacitance C_s, since the plasma area can be treated, in first approximation, as a virtual electrode extension, according to the schematic representation given in Fig. 9. Considering a relative permittivity $\varepsilon_r = 3.4$ for the plexiglas, this simplified approach leads to

$$C_s \cong \varepsilon_o \varepsilon_r \frac{(1\div 2)L \cdot W}{d} = 18 \div 36\ \text{pF} \tag{2}$$

The load capacitance has been also evaluated by using the finite element software Ansoft-Maxwell leading to values in the range 26.8–42 pF. These values are in good agreement with those calculated with the simplified approach (2), considering that neglecting the edge effects leads to slightly lower capacitance values.

The equivalent series resistance R_s, accounting for losses and conversion phenomena in plasma, is estimated on the basis of experimental active power measurements in the case of rectangular waveforms (Fig. 5a) as

$$R_s \cong \frac{P_{tot}}{I_{rms}^2} \cong 6\ \text{k}\Omega \tag{3}$$

The electric behavior of the DBD plasma actuator is strongly affected by the voltage waveforms during level transitions. In order to properly model rising and falling voltage transients in numerical simulations, detailed zooms of the experimental rectangular voltage waveform presented Fig. 5a are considered. In particular, Figs. 6a and 6b show the details of both voltage and current waveforms during negative and positive voltage transients (±14.4 kV), respectively. For both cases the transient time is about 0.75 µs, corresponding to a voltage rate of about 40 kV/µs. A proper third-order RLC circuit has been synthesized and tuned to adapt the ideal switching transients of the circuit simulator to the experimental behavior presented in Fig. 6.

The whole system, including the H-bridge multilevel inverter and the DBD plasma actuator, has been numerically implemented by the Simulink tool of Matlab, leading to the block diagram presented in Fig. 10.

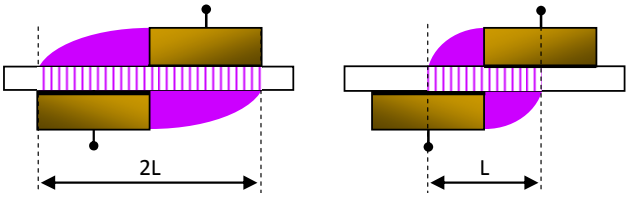

Fig. 9. Evaluation of virtual electrodes dimension due to plasma discharges.

This article has been accepted for publication in a future issue of this journal, but has not been fully edited. Content may change prior to final publication. Citation information: DOI 10.1109/TIA.2015.2409262, IEEE Transactions on Industry Applications

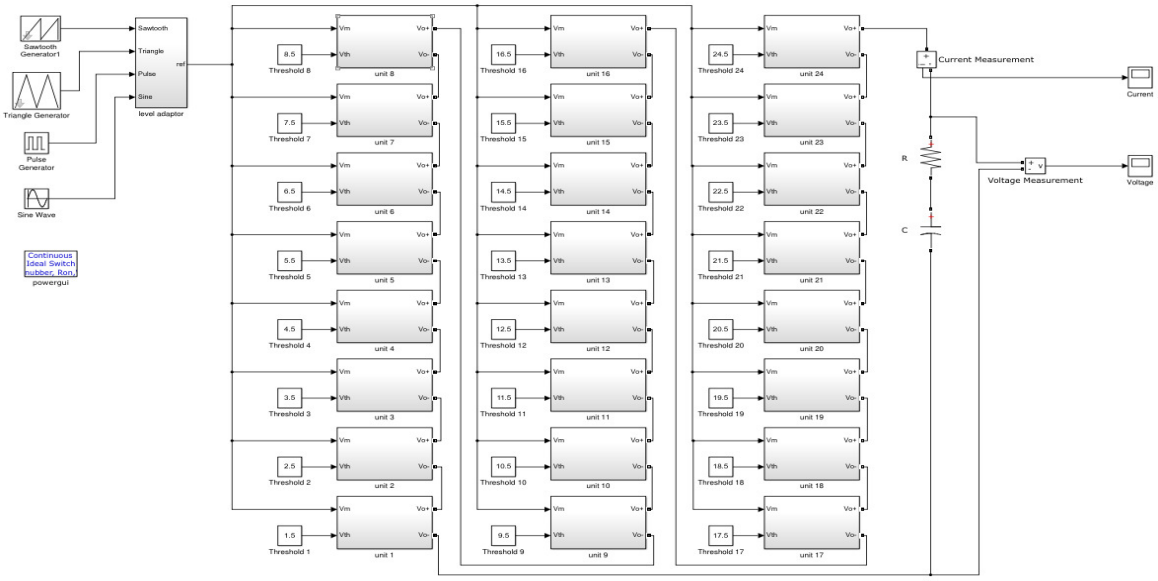

Fig. 10. Block diagram of the whole system model implemented by Simulink of Matlab.

In Fig. 11 are presented the simulation results considering the rectangular voltage waveform ±14.4 kV, corresponding to experimental results shown in Fig. 6. The circuit model parameters have been estimated by (2) and (3). In particular, a good matching for both voltage and current waveforms has been found by considering: C_s = 32 pF, R_s = 6 kΩ.

The same circuit model parameters have been adopted to simulate the triangular voltage waveform shown in Fig. 5b. The simulation results including rectangular and triangular voltage waveforms (5 kHz, ±14.4 kV) are presented in Fig. 12 (a) and (b), respectively. Also in these cases, the matching with experimental tests of both voltage and current wave-

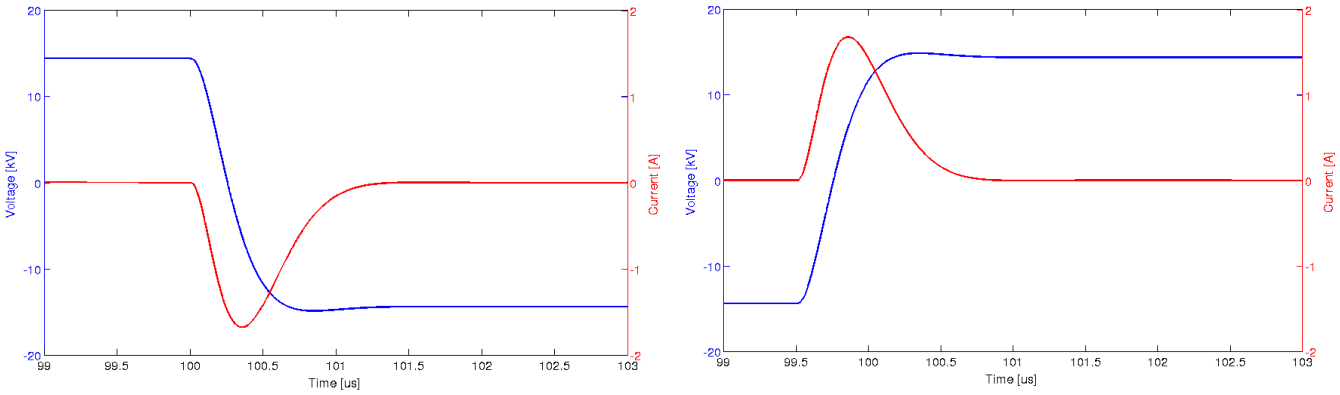

(a) (b)

Fig. 11. Simulation results: zoom of falling and rising voltage transients, (a) and (b), respectively, corresponding to the experimental results of Fig. 6.

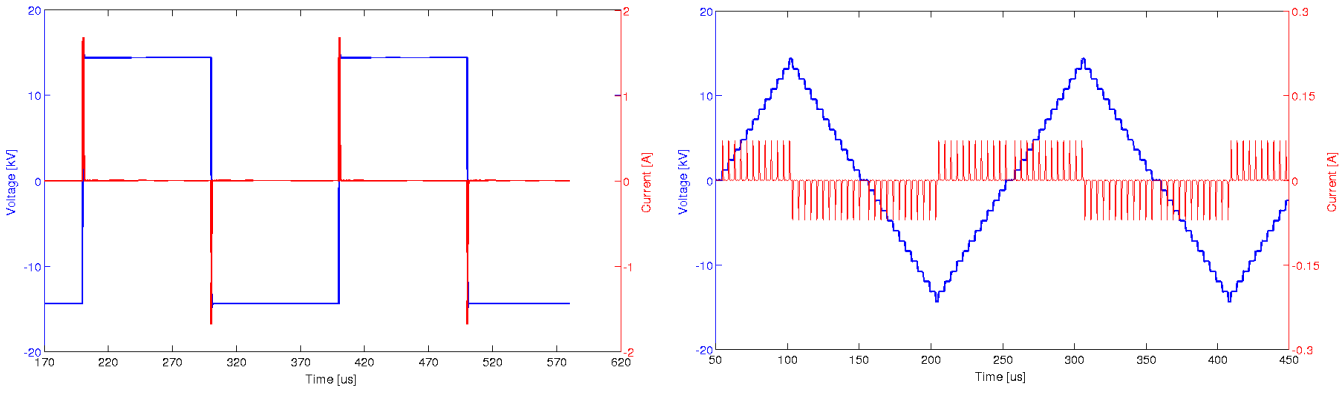

(a) (b)

Fig. 12. Simulation results: rectangular and triangular voltage waveforms, (a) and (b), respectively, corresponding to experimental results of Fig. 4.

forms is almost satisfactory, despite of the extremely simplified circuit model adopted for the DBD plasma actuator.

VI. Conclusions

A high-voltage high-frequency arbitrary voltage waveforms generator based on cascaded H-bridge multilevel topology has been designed, analyzed and experimentally realized. The converter configuration proposed in this paper is voltage-source type, and presents different advantages compared to traditional high-voltage high-frequency resonant generators. In particular, it can produce a wide set of different voltage waveforms, not just sinusoids, and it operates at frequencies independent by the load characteristics, having no impedance matching requirements. The multilevel generator has been designed with 24 insulated H-bridge modules, supplied by flyback converters and low-voltage batteries (dc sources), achieving simple and reliable high-voltage isolation and a portable device. It is capable of ±14.4 kV voltage waveforms with a frequency up to 20 kHz.

The generator has been realized and successfully tested by supplying a DBD fluid-dynamic plasma actuator with different voltage waveforms. Actuators with spanwise lengths in the range 0.1−1.5 m have been successfully fed, pointing out the absence of matching impedance requirements when using the multilevel generator. Output active power up to 320 W and efficiencies of about 66% have been measured and calculated. The proposed generator working in multilevel sinusoidal mode has been compared with a conventional AC sinusoidal generator, pointing out the possibility to supply the same power to the discharge but without any impedance matching requirement, and with an increased efficiency.

By the analysis of the experimental results, a simplified and effective circuit model of the DBD plasma actuator has been introduced. The whole conversion system has been numerically implemented by the Simulink tool of Matlab, obtaining simulation results in good agreement with the corresponding experiments.

VII. References

[1] C. Tendero, C. Tixier, P. Tristant, J. Desmaison, P. Leprince, "Atmospheric pressure plasmas: A review," *Spectrochimica Acta Part B: Atomic Spectroscopy*, vol. 61, No. 1, pp. 2-30, Jan. 2006.

[2] L. Bárdos, H. Baránková, "Cold atmospheric plasma: Sources, processes, and applications," *Thin Solid Films*, vol. 518, No. 23, pp. 6705-6713, Sept. 2010.

[3] A. Fridman, A. Chirokov and A. Gutsol. "*Non-thermal atmospheric pressure discharges,*" *J. Phys D: Appl Phys*, 38: R1-R24, 2005.

[4] U. Kogelschatz. "Atmospheric-pressure plasma technology". *Plasma Phys. Control. Fusion*, vol 46, issue 12B, B63-B75, 2004.

[5] J.Y. Jeong, S. E. Babayan, V. J. Tu, J. Park, I. Henins, R. F. Hicks and G. S. Selwyn.. "Etching materials with an atmospheric pressure plasmas jet". *Plasma Sources Sci Technol*, 7: 282-285, 1998.

[6] N. Yaman, E. Özdoğan, and N. Seventekin, "Atmospheric plasma treatment of polypropylene fabric for improved dyeability with insoluble textile dyestuff", *Fibers and Polymers*, February 2011, Vol. 12, No. 1, pp. 35-41.

[7] S. Lerouge, M.R. Wertheimer and L'H. Yahia "Plasma Sterilization: A Review of Parameters, Mechanisms, and Limitations," *Plasmas and Polymers*, Vol. 6, No. 3, Sept. 2001.

[8] M. Been Chang, C. Chun-Cheng, "Destruction and removal of toluene and MEK from gas streams with silent discharge plasmas", *American Inst. of Chemical Engineers. AIChE Journal*; May 1997; 43, 5; pg. 1325

[9] G.J. Pietscha and V.I. Gibalovb "Dielectric barrier discharges and ozone synthesis," *Pure&Appl. Chem*.,Vol.70, No. 6, pp. 1169-1174,1998.

[10] S. Min, G.A. Evrendilek, H.Q. Zhang, "Pulsed Electric Fields: Processing System, Microbial and Enzyme Inhibition, and Shelf Life Extension of Foods," *IEEE Trans. on Plasma Science*, vol. 35, No. 1, pp. 59-73, Feb. 2007.

[11] A. H. El-Hag, S. H. Jayaram, M.W. Griffiths, "Inactivation of Naturally Grown Microorganisms in Orange Juice Using Pulsed Electric Fields," *Plasma Science, IEEE Transactions on*, vol. 34, iss. 4, pt. 2, pp. 1412-1415, Aug. 2006

[12] M. Laroussi, "Low Temperature Plasma-Based Sterilization: Overview and State-of-the-Art," *Plasma Processes and Polymers*, vol. 2, iss. 5, pp. 391-400, Jun. 2005.

[13] G. Friedman, A. Gutsol, A.B. Shekhter, V.N. Vasilets, A. Fridman, "Applied Plasma Medicine", *Plasma Processes and Polymers*, Vol. 5, Issue 6, Article first published online: 16 Apr. 2008.

[14] T.C. Corke, C. Lon Enloe, S. P. Wilkinson, "Dielectric Barrier Discharge Plasma Actuators for Flow Control," *Annual Review of Fluid Mechanics*, vol. 42, pp. 505-529, 2010.

[15] N. Benard, E. Moreau, "Role of the electric waveform supplying a dielectric barrier discharge plasma actuator," *Applied Physics Letters*, vol. 100, No. 9, ref. 193503, May 2012.

[16] A. Cristofolini, C.A. Borghi, and G. Neretti, "Charge distribution on the surface of a dielectric barrier discharge actuator for the fluid-dynamic controll," *J. of Appl. Phys*. 113, 143307 (2013).

[17] A. Cristofolini, G. Neretti, and C. A. Borghi, "Effect of the charge surface distribution on the flow field induced by a dielectric barrier discharge actuator," *J. Appl. Phys*. 114, 073303 (2013).

[18] J. Rodriguez, S. Bernet, Bin Wu, J. O. Pontt, "Multilevel Voltage-Source-Converter Topologies for Industrial Medium-Voltage Drives," *IEEE Trans. on Industrial Electronics*, vol. 54, no. 6, pp. 2930-2945, Dec. 2007.

[19] M. Hagiwara, K. Nishimura, and H. Akagi, "A Medium-Voltage Motor Drive With a Modular Multilevel PWM Inverter," *IEEE Trans. on Power Electronics*, vol. 25, no. 7, July 2010.

[20] H. Mohammadi P. and M. Tavakoli Bina, " A Transformerless Medium-Voltage STATCOM Topology Based on Extended Modular Multilevel Converters," *IEEE Trans. on Power Electronics*, vol. 26, no. 5, p. 1534, May 2011.

[21] M. Veenstra and A. Rufer, "Control of a Hybrid Asymmetric Multilevel Inverter for Competitive Medium-Voltage Industrial Drives," *IEEE Trans. on Industry Applications*, vol. 41, no. 2, p. 655, March/April 2005.

[22] T. Boller, J. Holtz, and A.K. Rathore, "Neutral-Point Potential Balancing Using Synchronous Optimal Pulsewidth Modulation of Multilevel Inverters in Medium-Voltage High-Power AC Drives," *IEEE Trans. on Industry Applications*, vol. 50, no. 1, p. 549, Jan/Feb 2014.

[23] Md.R. Islam, Y. Guo, and J. Zhu, "A High-Frequency Link Multilevel Cascaded Medium-Voltage Converter for Direct Grid Integration of Renewable Energy Systems," *IEEE Trans. on Power Electronics*, vol. 29, no. 8, p. 4167, Aug. 2014.

[24] Mitsubishi Electric, "Dual-In-Line Package Intelligent Power Module," *PS22A74 datasheet*, Jan. 2012.